Exp Biol Med (Maywood) OnlineFirst, published on March 5, 2014 as doi:10.1177/1535370214522588

Original Research

Autocrine inhibition of the c-fms proto-oncogene reduces breast cancer bone metastasis assessed with *in vivo* dual-modality imaging

Justin J Jeffery[1], Katie Lux[2], John S Vogel[1], Wynetta D Herrera[3], Stephen Greco[2], Ho-Hyung Woo[2], Nisreen AbuShahin[2,4], Mark D Pagel[1,2,3] and Setsuko K Chambers[2]

[1]Department of Biomedical Engineering, University of Arizona, Tucson, AZ 85721, USA; [2]University of Arizona Cancer Center, Tucson, AZ 85724, USA; [3]Department of Chemistry and Biochemistry, University of Arizona, Tucson, AZ 85721, USA; [4]Department of Pathology, University of Jordan, Amman, 11942, Jordan

Corresponding author: Setsuko K Chambers. Email: schambers@uacc.arizona.edu

Abstract

Breast cancer cells preferentially home to the bone microenvironment, which provides a unique niche with a network of multiple bidirectional communications between host and tumor, promoting survival and growth of bone metastases. In the bone microenvironment, the c-fms proto-oncogene that encodes for the CSF-1 receptor, along with CSF-1, serves as one critical cytokine/receptor pair, functioning in paracrine and autocrine fashion. Previous studies concentrated on the effect of inhibition of host (mouse) c-fms on bone metastasis, with resulting decrease in osteolysis and bone metastases as a paracrine effect. In this report, we assessed the role of c-fms inhibition within the tumor cells (autocrine effect) in the early establishment of breast cancer cells in bone and the effects of this early c-fms inhibition on subsequent bone metastases and destruction. This study exploited a multidisciplinary approach by employing two non-invasive, *in vivo* imaging methods to assess the progression of bone metastases and bone destruction, in addition to *ex vivo* analyses using RT-PCR and histopathology. Using a mouse model of bone homing human breast cancer cells, we showed that an early one-time application of anti-human c-fms antibody delayed growth of bone metastases and bone destruction for at least 31 days as quantitatively measured by bioluminescence imaging and computed tomography, compared to controls. Thus, neutralizing human c-fms in the breast cancer cell alone decreases extent of subsequent bone metastasis formation and osteolysis. Furthermore, we are the first to show that anti-c-fms antibodies can impact early establishment of breast cancer cells in bone.

Keywords: C-fms proto-oncogene, breast cancer, bone metastasis, osteolysis, autocrine

***Experimental Biology and Medicine* 2014; 0: 1–10. DOI: 10.1177/1535370214522588**

Introduction

The propensity of breast cancer cells to invade and metastasize early, prior to clinical detection, is the primary determinant of poor outcome. This cancer, more so than most solid tumors, has the predilection to spread to bone resulting in bone destruction. Bone-seeking breast cancer cells enhance osteolysis of bone,[1–5] while the bone tumor microenvironment in turn stimulates the growth of the tumor cells and alters their phenotype, promoting a vicious cycle of metastasis and bone pathology.[6] Breast cancer patients with bone spread, while largely incurable, can live many years, while suffering consequences of bone metastases. Ultimately, 70% of those patients will develop skeletal complications from the associated bone destruction including fractures, immobilization and loss of independence, and bone pain, severely impacting their quality of life.[7] Thus, there is a need to better understand mechanisms regulating the bone-seeking nature of breast cancer cells, and approaches to prevent or inhibit these bone metastases.

Our laboratory and others have been studying the regulation of breast cancer metastasis by the c-fms proto-oncogene, which is expressed by the large majority of breast cancers but not by normal tissues, except for macrophages and osteoclasts. Elevated c-fms levels in the breast cancer specimens confer increased risk for local relapse[8] and poor survival of breast cancer patients,[9] with new regulators of c-fms expression being described.[10,11] C-fms is activated by autocrine and paracrine CSF-1 signaling, conferring an invasive metastatic phenotype.[12–15] The majority of breast cancer cells express c-fms with one-third co-expressing

CSF-1, thus allowing for autocrine interactions.[16–18] We and others have described the role of the autocrine loop between c-fms and CSF-1 in breast cancer cells as important to both *in vitro* and *in vivo* invasion and metastasis.[15–21] In addition, tumor-associated macrophages bearing CSF-1 promote progression of primary breast cancer in a paracrine manner.[22–26] For instance, in mice bearing human breast cancer xenografts not expressing c-fms, targeting mouse (host) c-fms or CSF-1 suppressed primary tumor growth by 40–50%[27,28] and improved their survival.[28]

In the bone environment, binding between CSF-1 and c-fms is also essential for differentiation and activation of osteoclasts.[3,4,29] Breast cancer cells secreting CSF-1 can increase osteoclast formation in the presence of bone stromal cells.[3] CSF-1 can also regulate osteoclast motility and survival,[4] and mutations in c-fms confer impaired osteoclast differentiation and bone resorption.[5] Thus, c-fms related autocrine and paracrine interactions between and within the tumor cells and bone environment may contribute to the bone-seeking phenotype of breast cancer cells that express c-fms and CSF-1, and to the triggering of bone destruction and pain by these metastases.

Targeting c-fms in a treatment strategy has great potential to reduce osteolysis. The inhibition of the paracrine role of activated c-fms signaling has been studied in bone metastases from breast cancer cells.[30–33] Using tumor cells that do not express c-fms, therapeutic inhibition of host c-fms activity by anti-c-fms small molecule inhibitors (SMIs) reduced osteolysis and tumor volume within the bone. These SMIs included receptor tyrosine kinase inhibitors including Sunitinib[30] and Imatinib,[31] as well as specific c-fms inhibitors including JNJ-28312141.[32] Similarly, paracrine down-regulation of host c-fms by another SMI, Ki20227, reduced osteolysis from bone metastases derived from melanoma.[33]

To our knowledge and to date, there have been no studies of the effects of direct inhibition of autocrine c-fms activity in breast cancer cells on bone metastasis and bone destruction. In this study, we investigated if an anti-c-fms antibody therapy can inhibit autocrine c-fms signaling and affect subsequent establishment of bone metastases and bone destruction from breast cancer cells. We hypothesized that delivery of an anti-c-fms antibody targeted to breast cancer cells expressing c-fms and CSF-1 can interfere with the autocrine signaling of this bone-seeking phenotype, and such treatment can inhibit both extent of bone metastases and bone destruction. To investigate our hypotheses, we used an immunosuppressed mouse model wherein mouse CSF-1 in bone is unable to stimulate human c-fms. This ensured that c-fms/CSF-1 interactions on osteolysis must be due to autocrine signaling, which facilitates our assessments of inhibiting the autocrine pathway.

RT-PCR and histopathology techniques are commonly employed to assess the molecular and cellular changes during the progression and treatment of bone metastases. Yet, these analyses require serial sacrifice within a mouse model, which cannot track longitudinal progression. Furthermore, bone metastasis studies can greatly benefit from longitudinal evaluations of tumor growth as well as bone destruction, to evaluate the integrated functions of tumor cells and osteoclasts. Non-invasive imaging provides an outstanding paradigm for these longitudinal studies. More specifically, bioluminescence imaging (BLI) can rapidly track tumor growth, and micro-Computed Tomography (micro-CT) can assess bone morphology and volume with exceptional precision. We incorporated this dual-modality imaging approach into our studies of an experimental bone metastasis model to investigate whether a one-time early delivery of anti-human c-fms antibody can significantly reduce subsequent bone metastases and bone destruction.

Materials and methods

Bone homing human breast cancer cell line

Serial intracardiac (IC) injection of breast cancer cells is the most reliable method to isolate bone-homing cells for developing experimental bone metastasis models of human breast cancer.[30,34–37] We obtained such a bone homing MDA-MB-231-BO clone, courtesy of the Yoneda laboratory.[34] Cells were maintained in DMEM (Hyclone) supplemented with 0.1 mM non-essential amino acids, 2 mM L-glutamine, 1 mM sodium pyruvate, 1.5 g/L sodium bicarbonate, and 10% fetal calf serum (Invitrogen Inc., Carlsbad, CA, USA) in 5% CO_2 at 37°C. We created stable transfectants of this clone with a thermostable luciferase bearing construct,[38] expressing luciferase for the *in vivo* imaging experiments. We have characterized these cells to secrete >2-fold more CSF-1 than the parent cells, with comparable levels of c-fms protein.

Mouse imaging model of bone metastasis from breast cancer

All studies with mice were conducted with prior approval of the Institutional Animal Care and Use Committee of the University of Arizona, following internationally recognized guidelines. We utilized the IC experimental bone metastasis model[34] with MDA-MB-231-BO-luc cells modified as described. For all mouse experiments, four-week-old female Balb C mice underwent IC injection with 1×10^5 cells on day 0. First, to establish the bone homing nature of these cells, eight mice were followed with serial BLI starting on day 5 until sacrifice on day 26. They were simultaneously followed serially with micro-CT scans to evaluate extent of bone destruction. Long bones were harvested for immunohistochemical analysis of metastases for activated c-fms expression, to verify that these cells retained functional c-fms *in vivo*.

Next, groups of three mice each received either 20 mg/kg of anti-human c-fms, or control antibody intravenously on day 0 before IC injection of cells. From the work of others using an experimental bone metastasis model, it is known that some breast cancer cells can home to bone as early as 1 h after IC injection.[39] This knowledge impacted the timing of antibody delivery in these models. This tool (non-humanized) mouse-derived anti-human c-fms antibody was chimerized to human IgG, and shared with us, courtesy of Roche Diagnostics GmbH, Mannheim, Germany. It had high species specificity for both binding to human c-fms and for its capacity to inhibit binding of CSF-1 to human

c-fms. The mice were sacrificed on day 7. Bones were harvested and frozen for RNA extraction.

Lastly, a group of nine mice received 20 mg/kg of anti-human c-fms, a group of seven mice received control antibody, and a group of five mice received no treatment intravenously on day 0 before IC injection of cells. These mice were followed by serial BLI between day 7 and either death or day 31. A subset was also imaged by serial micro-CT scans between day 7 and either death or day 26. Some mice, that appeared well, were followed for longer periods until sacrifice on day 40. Bones were harvested for immunohistochemical analysis of metastases for c-fms and activated, phosphorylated c-fms (p-fms) expression. These mouse experiments were carried out with the assistance of the Experimental Mouse and Imaging Shared Service of the University of Arizona Cancer Center.

RT-PCR of RNA extracted from bone

Mouse bones were harvested, frozen in liquid nitrogen, and then stored at −80°C. For RNA isolation, bones were ground and kept frozen using mortar and pestle, and stored at −80°C. RNA was isolated by using TRIzol Reagent (Ambion® Life Technologies, Inc., Grand Island, NY, USA) according to their protocol with an additional step of acid phenol:chloroform extraction. RNA was dissolved in DEPC-treated water and concentration was determined using a BioRad SmartSpec3000 spectrophotometer. One microgram of RNA was reverse transcribed using first strand cDNA synthesis with M-MLV (Promega Corp., Fitchburg, WI, USA). One microliter of cDNA was used for amplification using Taq DNA polymerase kit (Fermentas Inc. Vilnius, Lithuania). The PCR cycle for all reactions was maintained at 95°C for 15 s, at 60°C for 15 s, and at 72°C for 30 s, with the number of cycles being either 35 or 40. PCR was carried out for luciferase and for mouse GAPDH, with primers for luciferase and mouse GAPDH being: forward- GACCAACG CCTTGATTGACAAGG, reverse- GACTGGCGACGTAAT CCACGATC, and forward-GCAGGCATCTGAGGGCCC ACTG, reverse-CAGTGTTGGGGGCCGAGTTGGGAT, respectively. Aliquots of 10 μL were analyzed using a 1% agarose gel. Intensities of the resulting bands were then used to determine a normalized percent intensity of luciferase relative to GAPDH. The comparisons between groups were performed using two-tailed *t*-test assuming equal variances among groups.

Bioluminescence Imaging

All mice were monitored by serial BLI twice weekly. Initial BLI studies that validated the tumor model were conducted using a VersArray 1300B camera (Roper Scientific, Inc., Trenton, NJ, USA) attached to a light-tight box. Scans were acquired with a 10-min exposure time, 1.2 f/stop aperture, and 25 cm field of view (FOV). All mice were injected intraperitoneally (IP) with 100 mg/kg firefly luciferin 10 min before acquisition. Four minutes after injecting luciferin, mice were injected IP with a cocktail consisting of ketamine and xylazine. Mice were oriented in a supine position in the scanner. Subsequent longer-term BLI studies that evaluated antibody treatments used an AMI1000 optical imaging scanner (Spectral Instruments Imaging, Inc., Tucson, AZ, USA) and AMI View software for acquisition and analysis. Scans were acquired with 30 s exposure time, high eight-fold binning, 1.2 f/stop aperture, and 25 cm FOV. All mice were injected IP with 100 mg/kg firefly luciferin 10 min before acquisition. Four minutes after injection, mice were inoculated with 4% isoflurane gas at 1 L/min oxygen flow and sedation was maintained during imaging with 1.5% isoflurane gas at 0.5 L/min oxygen flow.

Significant differences in bioluminescent signal occurred among all mice before and after day 24 of imaging, and consequently different upper and lower thresholds were used for images acquired between days 14 and 21 relative to images acquired between days 24 and 31 to appropriately scale the photon counts to maximize signal and limit background noise.[40] Regions of interest (ROIs) with identical size were carefully placed around the lower extremities to incorporate all bioluminescent signal at the appropriate threshold, while minimizing scatter signal. Radiance units were used for relative comparison of the sum of photons between scans.

MicroCT

Four mice in each group were also longitudinally imaged using micro-CT as a complimentary measure of c-fms inhibition on bone metastases. Micro-CT provides more specificity of tumor sites within regions including the bilateral femurs, which yields a more compelling visual and quantitative analysis of bone destruction.[41] The left and right femurs were analyzed independently so that each study group consisted of eight bones. The imaging was performed using a Inveon micro-CT scanner and Inveon Acquisition Workplace software, and Inveon Research Workplace 3D Visualization analysis software (Siemens Medical Solutions USA, Inc., Knoxville, TN, USA). All scans were acquired with the following parameters: 80 kVp, 2 s exposure time, 400 μA current, 45 micron focal spot size, 220 rotation steps with 401 projections that created a projection every 0.55°, ~17.5 min scan time, 0.5 mm aluminum filter, two-fold bin factor, and magnification that yielded an overall reconstructed isotropic voxel size of ~44 microns.

Scans were reconstructed with filtered back-projection and no down-sampling using integrated high-speed COBRA reconstruction software (Exxim Computing Corporation, Pleasanton, CA, USA). A scalar linear attenuation coefficient in Hounsfield Units (HU) was applied to each data-set to facilitate inter-scan comparisons. Three-dimensional images were segmented using a minimum pixel intensity of 900 HU, and a maximum intensity that was selected to represent bone density in a specific image.[42] To optimize objectivity, each analysis was independently conducted by two mouse imaging experts and results were averaged.[43] These analyses isolated the entire femur (plus the patella) from the acetabulum of the pelvis, tibia, and fibula, and subsequently measured femur volume and femur length.

For each treatment group, the average femur volume on each measurement day was normalized to the average femur volume measured on day 7 to assess the relative

change in femur volume over time. Similarly, the average ratio of femur volume to femur length was normalized to this ratio measured on day 7. The comparisons of these measurements between groups were performed using two-tailed *t*-test assuming equal variances among groups.

Immunohistochemistry

Bones were decalcified and H&Es of paraffin fixed sections were verified to contain breast cancer metastases by the Tissue Acquisition and Cellular/Molecular Analysis Shared Service of the University of Arizona Cancer Center. Immunohistochemistry was performed using the streptavidin-biotin-peroxidase technique with rabbit polyclonal antibodies for expression of c-fms (ab61137, 1:50 dilution; Abcam, Inc.), of p-fms (ab111334, 1:85 dilution; Abcam, Inc., Cambridge, UK) and of CSF-1 (ab9693.1:200 dilution; Abcam, Inc., Cambridge, UK) overnight at 4°C in a humidity chamber. Citrate buffer (pH 6.0) and a pressure cooker were for used for antigen retrieval. Endogenous peroxidase and nonspecific protein binding was blocked by 3% H_2O_2 in methanol, or 5% goat serum (Vector Laboratories, Inc., Burlingame, CA, USA), respectively. Degree of staining (intensity and percent of slide stained) was scored separately for tumor and host tissue by a pathologist (NA) and trained scorer (KL), as described previously.[44]

Results

Breast cancer bone metastasis imaging model

Serial BLI was performed using the thermostable luciferase expressing MDA-MB-231-BO cells, in eight mice between days 5 and 26 (Figure 1). All eight mice (100%) developed bone metastases. At sacrifice on day 26, no gross tumor was noted in lung, brain, liver, or ovaries, as expected in this bone-homing tumor model. No bioluminescence was observed on day 5 in any of the mice. Light was detected for the first time in some mice starting on day 7, while light was initially detected in the other mice on day 12 or 14. Eventually widespread bone metastases were detected in this mouse model. We have learned through similar studies with this mouse model that the onset of detectable bone metastasis can show some variability between experiments with different aliquots of cells. However, conditions can be reliably compared within an experiment using a single aliquot of cells.

Micro-CT scans of the left femur and tibia were also obtained in mice at matching time points starting on day 14. Similar to the BLI results, micro-CT detected the formation of osteolytic lesions in the left tibia starting on day 14 (Figure 1). The micro-CT scans show increasing bone destruction over time in this location, and similar destruction in the iliac crest and femur (not shown). The metastases from this breast cancer cell line were osteolytic, representative of the majority of human breast cancer bone metastases. MDA-MB-231-BO tumor cells may have been affected by radiation during micro-CT scanning, even though the dose of radiation generated by micro-CT is extremely low relative to traditional radiotherapy. However, the evidence of increasing bone destruction during the longitudinal study with periodic micro-CT scanning indicated that this breast cancer cell line still retained an osteolytic phenotype despite any possible radiation effects caused by micro-CT. CT scans were more precise at determining anatomic location of sites of tumor/bone destruction than BLI. For example, in this mouse on day 26, the micro-CT scan of the lower half of the body delineated osteolytic lesions associated with metastases in the right femur, left femur, left tibia, bilateral iliac crests, and bilateral pubic bones. For comparison, the photon counts from the various regions had overlapped and merged by this time point, obviating the

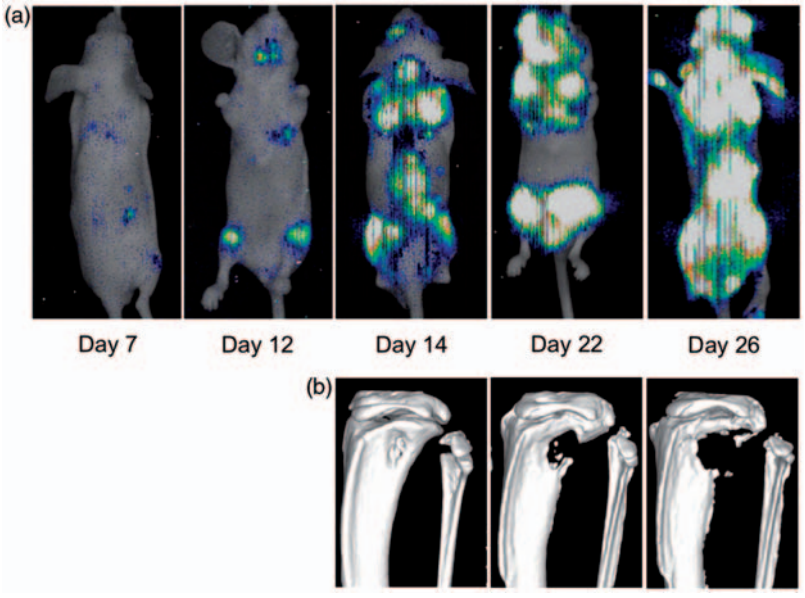

Figure 1 Imaging model of bone metastasis from breast cancer. (a) Serial bioluminescence imaging from day 7 through day 26 after intracardiac injection of MDA-MB-231-BO-luc cells showed growth of bone metastases including tumor growth in the femur and/or tibia. (b) MicroCT imaging of the left tibia of the same mouse from days 14 to 26, showing increasing bone destruction from osteolytic metastasis. (A color version of this figure is available in the online journal.)

determination of the exact locations of the tumors. The BLI can be used to quantitatively assess rate of growth of metastases, while concurrent CT scanning can quantitatively detail the extent of associated bone destruction.

Effect of one-time anti-c-fms antibody on early establishment of bone metastases

We sought to determine the effect of a one-time injection of anti-human c-fms antibody on establishment of bone metastases from c-fms and CSF-1 expressing human breast cancer cells. We applied the anti-human c-fms antibody with species specificity, which should selectively inhibit c-fms on human breast cancer cells, thereby inhibiting autocrine c-fms/CSF-1 signaling. Luciferase RNA expression was detected from RNA extracted from bone at day 7 after IC injection of cells in a cohort of mice (Figure 2). This finding agrees with the work of others[39] suggesting that other breast cancer cells have the ability to home to bone as early as 1 h after IC injection, with growth of small foci (2–10 cells each) seen by day 7. Here, the effect of anti-human c-fms antibody was seen on significant inhibition of luciferase RNA expression by day 7 ($P < 0.01$). These experiments were designed to study the effect on early establishment of bone metastases from breast cancer cells, but could not differentiate between effects on bone homing, implantation, or cancer cell survival in the bone microenvironment. Yet, these experiments suggest, for the first time, that down-regulating the c-fms/CSF-1 autocrine loop in these cells reduces the early establishment of bone metastases.

Long-term follow-up of the effect of the one-time injection of the anti-human c-fms antibody on bone metastases and bone destruction

Since there was a clear effect on extent of early bone metastasis establishment by breast cancer cells from our anti-c-fms strategy, we performed a long-term experiment where the mice were followed for 26 days with micro-CT and 31 days with BLI, and then followed to assess survival for up to 40 days (Figure 3). Three groups of 5–9 mice were tested during BLI studies. Due to the longer time required for micro-CT scanning, only four mice per group were imaged with micro-CT. However, this analysis provided eight tibias and femurs per group, which facilitated the statistical analyses of the imaging results. The BLI results demonstrated a lag in growth, along with inhibition of extent of bone metastasis as assessed by photon emission. A significant difference between the control antibody and anti-c-fms antibody groups was seen on day 31 (Figure 3b). In fact, five of nine mice who received anti-c-fms antibody never achieved photon emissions over 1×10^8 photons.

We complemented these studies by performing serial micro-CT scans on four mice from each group (Figure 4). The pelvis and lower extremities were chosen as regions of focus. Evident by this approach was the significant lag in bone destruction over time as demonstrated by the mice that received the anti-human c-fms antibody. The untreated and control groups developed evidence of bone destruction as early as day 19. After the one-time preventive treatment with anti-human c-fms antibody, one mouse developed bone destruction very late in follow-up (day 33). Another mouse, which never demonstrated significant photon emission, also never developed bone destruction as assessed by micro-CT prior to sacrifice on day 40.

To quantitatively assess the micro-CT results, we exhaustively evaluated the volume and length of each femur using 3D segmentation (Figure 5). Inter-observer agreements of these evaluations were outstanding due to only a single subjective variable remaining in the procedure (the determination of the maximum threshold of bone density). Each femur was discovered to have a different bone volume on day 7. Because BLI did not detect significant bone metastases by day 7, we attributed these different bone volumes to minor differences in overall growth status for each mouse. To account for these differences, the average femur volumes measured on subsequent days were normalized to the average femur volume on day 7 for each treatment group (Figure 6a). There was a significant difference detected by day 26 between the groups treated

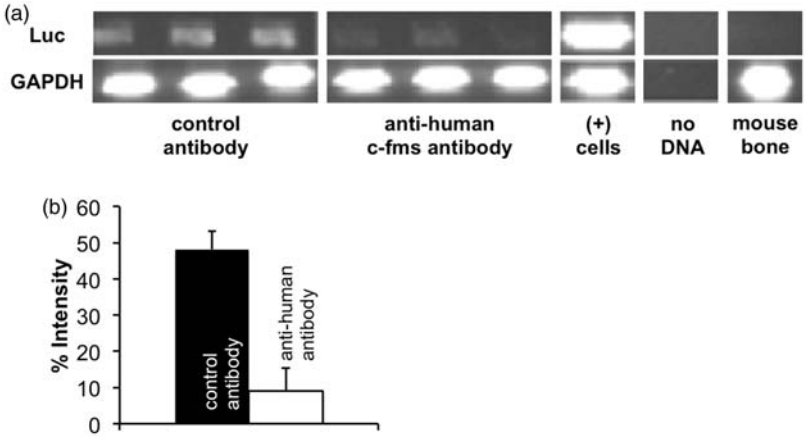

Figure 2 (a) RT-PCR of luciferase RNA expression in the right humerus of each mouse at day 7. Mouse GAPDH was used as a measure of amount of host tissue. (b) Luciferase and mouse GAPDH RNA were quantified using densitometry. The normalized % intensity of luciferase RNA relative to mouse GAPDH showed that luciferase was highly expressed in bones of mice that received the control antibody, and treatment with anti-human c-fms antibody significantly reduced luciferase expression

with anti-human c-fms antibody and control antibody ($P < 0.05$).

As a potential pitfall, continuous overall growth of each mouse may cause femur volumes to increase, which would offset a decrease in bone volume caused by the formation of osteolytic lesions, which would reduce the statistical significance of differences between treatment groups. To address this pitfall, we hypothesized that femur length is a quantitative biomarker of femur growth that is not influenced by the formation of osteolytic lesions (lesions did not form at the end of the femur, as evidenced by micro-CT images). Therefore, the ratio of femur volume to femur length should be a more sensitive measurement of the formation of osteolytic lesions. We evaluated the average of the ratio of volume-to-length for each femur, and normalized each result to the average femur volume-to-length measurement determined on day 7 for each treatment group (Figure 6b). We found that this normalization successfully detected statistically significant differences on day 26 in the group treated with anti-human c-fms antibody relative to both control groups: those treated with the control antibody or the untreated group ($P < 0.05$).

These results suggest that neutralizing c-fms on the human breast cancer cell by a simple one-time antibody-based approach may impact significantly on growth rate of bone metastases and on extent of bone destruction.

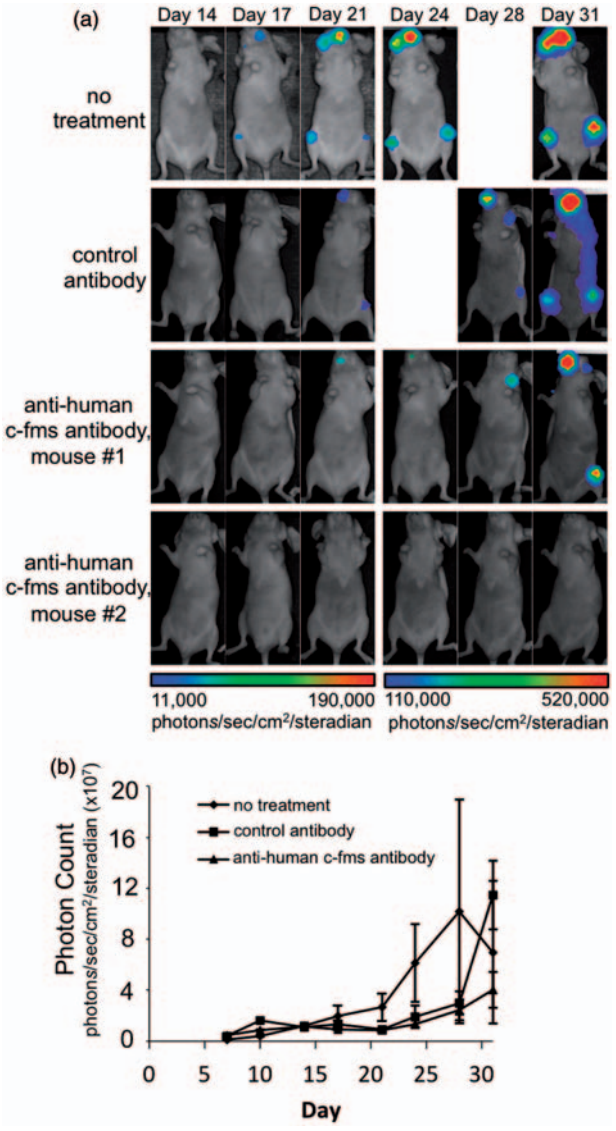

Figure 3 (a) Serial bioluminescence images of the effects of one-time application of anti-human c-fms antibody. Bioluminescence imaging was performed of mice from days 7 to 31, and representative mice are depicted from each group. Only images acquired from days 14 to 31 are shown, because images acquired from day 7 to day 11 showed negligible bioluminescence. Images acquired between day 14 and day 21 are scaled differently relative to images acquired between day 24 and day 31, as shown by the scale bars at the bottom of the panel of images, to improve visualization of low bioluminescence at the earlier time points. Untreated mice showed measureable light at day 17, with substantial growth of metastases at day 31. Mice treated with control antibody also showed metastasis at day 31, although the level of metastasis was less than metastases detected in untreated mice. Mice treated with anti-human c-fms antibody emitted the least amount of light over time, and five of the nine mice in this treatment group had negligible light emission. (b) The measurement of the mean photon count (±SEM) taken from bilateral femurs over time for each of the three groups showed a significant difference between the control antibody and anti-human c-fms antibody group on day 31 ($P < 0.05$)

c-fms expression in bone metastases

Immunohistochemical analysis for expression of c-fms, p-fms, and CSF-1 was performed on the bone metastases (Figure 7). These metastases represent those that survived

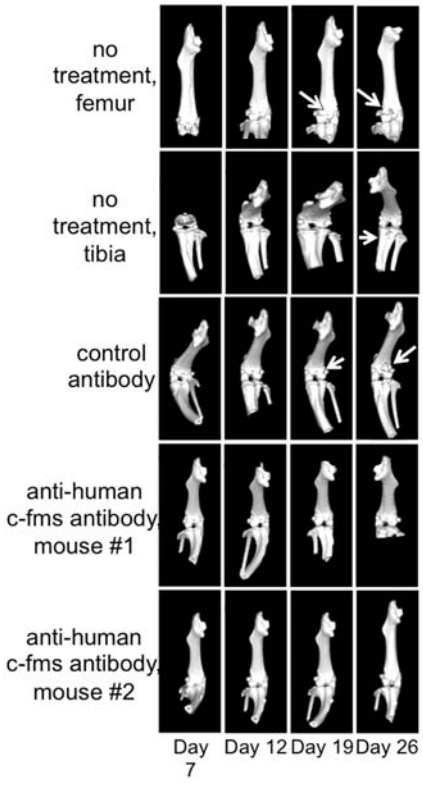

Figure 4 Serial micro-CT images of the effects of application of one-time anti-human c-fms antibody. Micro-CT imaging was performed of mice from days 7 to 26, and the same mice as in Figure 3 are depicted from each group. Untreated mice showed osteolytic lesions as early as day 19. Mice treated with control antibody also showed osteolytic lesions at day 19. Mice treated with anti-human c-fms antibody either showed osteolytic lesions at later time points, or showed no evidence for osteolytic lesions

our intervention on day 0. All evaluated tumor metastases in bone strongly expressed c-fms in 95% of cells, with no difference between groups. P-fms was expressed with less intensity in general, but in 75–90% of tumor cells, again with no difference between groups. Stromal cells within the tumor also occasionally expressed both c-fms and p-fms. Host bone marrow cells expressed c-fms strongly, more than p-fms. The bone matrix was negative for any staining. Thus, the bone metastases retained expression of c-fms, capable of being activated by CSF-1, suggesting that they remain susceptible to intervening anti-c-fms treatment. CSF-1 staining was present in both tumor and stroma serving as autocrine and paracrine sources for activation of c-fms. No difference in CSF-1 staining was seen between groups, as expected.

Survival

While the mouse experiments were not powered for survival analysis, it is notable that only three of seven mice from the control antibody group remained alive on day 40 (day of sacrifice), compared to seven of nine mice from the anti-human c-fms antibody group. This result suggests that the one-time antibody strategy employed in these studies may impact favorably on long-term survival, although additional studies are warranted to confirm this preliminary result.

Figure 5 Quantitative processing of micro-CT images. (a) A 3D segmentation identified the exterior of the femur including the femoral head and excluding the acetabulum of the pelvis, tibia, and fibula. (b) Additional segmentation identified voids within the bone. Expanded views of the proximal femur (top) and distal femur (bottom) are shown. (c) The fully segmented volume was used to determine femur volume and length

Discussion

Paracrine c-fms signaling has previously been shown to be one of several important communication networks within the breast cancer bone environment. Our report is the first to show that autocrine signaling is important for early establishment of bone metastasis from breast cancer cells. We are the first to evaluate an anti-c-fms approach on breast cancer cell establishment in the bone, and that targeting autocrine c-fms/CSF-1 signaling on breast cancer cells reduces bone metastasis and bone loss. These new results add to prior reports of efficacy of targeting c-fms in the host environment of established breast cancer bone metastases. Our preclinical work suggests that there would likely be a clinical benefit through neutralizing c-fms on the tumor cell, simultaneously with neutralizing c-fms in the host environment, which would result during the treatment of patients.

Previous reports[30–33] have applied specific or non-specific anti-c-fms SMIs targeted to study the treatment of established breast cancer bone metastases. To our knowledge, our report is the first to utilize a neutralizing anti-c-fms antibody in the study of breast cancer bone metastasis. The species-specificity of the antibody allowed us to study the effect of targeting tumor cells only, separate from that of the host tissue, which ensured that our results were specific only to autocrine signaling. Yet, our

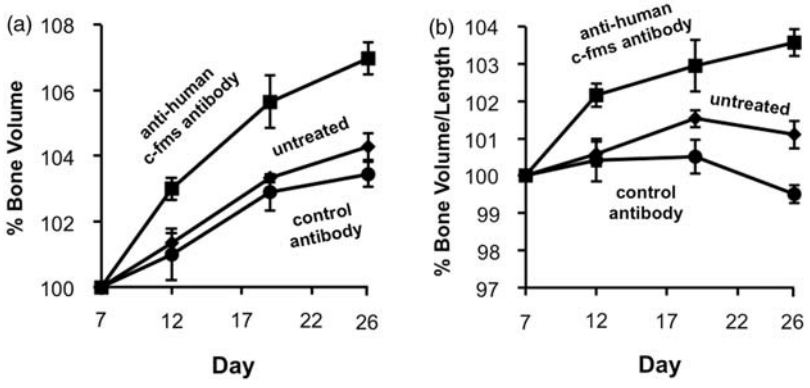

Figure 6 Quantitative analysis of micro-CT imaging following the one-time application of anti-human c-fms antibody. (a) The average bone volume (± SEM) was normalized relative to results on day 7. The normalized bone volumes on day 26 were significantly different ($P < 0.05$) for the anti-human c-fms treatment group relative to the control antibody treated group, but was not significantly different relative to the untreated group. (b) The average ratio of the bone volume to length (±SEM) was normalized relative to results on day 7. For results on day 26, this measure for the anti-human c-fms treatment group was significantly different relative to both the untreated and control antibody-treated groups ($P < 0.05$)

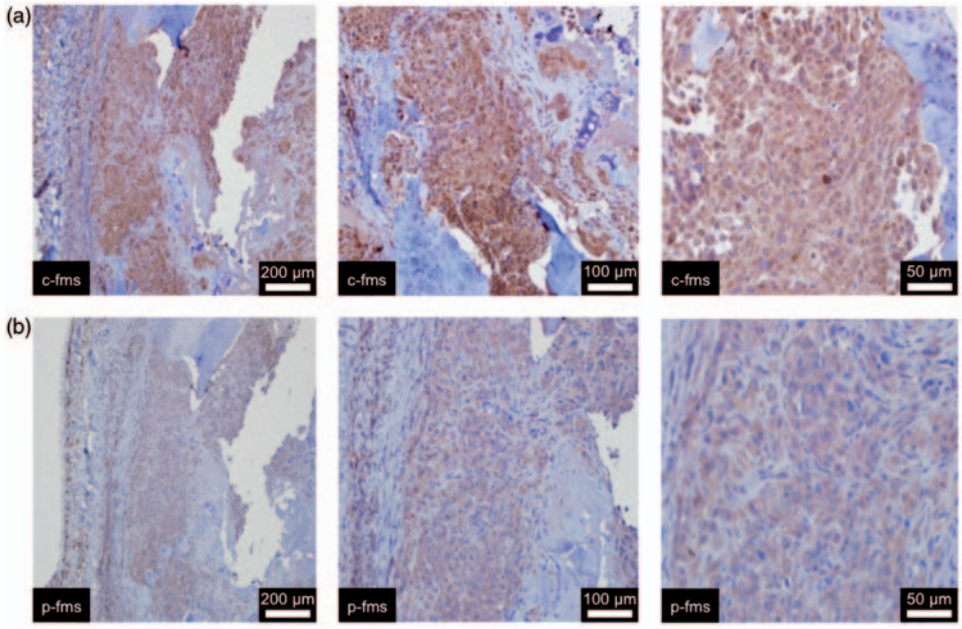

Figure 7 Expression of total and activated c-fms in a representative bone metastasis by immunohistochemistry. The tumor involved the bone marrow and invaded bone. (a) c-fms expression with 3+ intensity, 95% in tumor cells and 2+ intensity, 40% in the stromal cells within the tumor. (b) Activated phosphorylated c-fms (p-fms) expression with 2+ intensity, 75% in the tumor cells and 3+, 30% in the stromal cells

experiments cannot distinguish the precise mechanism for our early effect of the anti-c-fms antibodies on inhibition of establishment of breast cancer cells in bone. Rate-limiting steps between circulating tumor cells and their establishment in bone include survival in the bloodstream, extravasation, and adhesion/survival in bone, followed by subsequent growth. Future studies of the effect of c-fms inhibition on these specific steps may further elucidate these mechanisms.

It is clear from the work of others[45,46] that c-fms bearing macrophages are critical to the intravasation process of breast tumor cells, and thereby extent of circulating tumor cells, as well as promoting extravasation, survival, and persistent growth of these cells.[46] We hypothesize that the anti-human c-fms antibody may interfere with function of both circulating tumor cells, as well as those which have seeded the bone marrow. Reduction of CSF-1 secreting breast tumor burden in bone in this manner would lead to a relative decrease in CSF-1 in the environment. Such a decrease could contribute to the inhibition of osteolysis observed in our study.

The durability of the early one-time anti-c-fms antibody approach was surprising. The reduction in rate of growth of subsequent bone metastases coupled with decrease in bone destruction lasted for up to 40 days. Translating to patients, early seeding of the bloodstream and distant organs, such as the bone, appears to occur with invasion of the primary tumor. Thus, by the time the tumor is diagnosed, metastatic microfoci likely already exist in many cases. However, after the primary tumor is resected, these metastatic foci can serve as a source for further seeding of the bloodstream and other metastatic sites. Therefore, the principle of secondary prevention/inhibition of bone metastases suggests an important clinical relevance. In patients, preventive methodologies frequently require repetitive or chronic treatment for long time periods. The durability of the antibody effect suggests that intermittent treatments may be sufficient. Furthermore, we found that bone metastases that survived in the bone environment still retained c-fms expression, even in mice that received anti-c-fms antibody treatment. This finding suggests that a therapeutic anti-c-fms approach may be effective in the clinic. Future studies are warranted to confirm these results using other models and in clinical studies.

We demonstrated the merits and limitations of *in vivo* imaging studies of bone metastases in this multidisciplinary study.[47] BLI is a rapid and inexpensive method for tracking bone metastases over a wide dynamic range of tumor load (Figure 3a). However, BLI suffers from poor spatial image resolution, and could not distinguish metastatic tumors in the femur relative to the tibia. BLI also cannot measure the extent of bone destruction from the tumors. The BLI results suffer from substantial variability, which negatively impacts the statistical comparisons of treatment groups over time (Figure 3b). In our study, this variability caused a statistical difference only for one late time point, and only between two of the three treatment groups. Micro-CT provides many advantages for assessing bone metastases, including 3D imaging and high spatial resolution (Figure 4) that can be used to accurately quantify the extent of osteolysis in the femur and tibia (Figure 5). In our study, this improved image quality was exploited to detect a statistically significant difference in bone volume as an inverse surrogate for measurement of extent of bone destruction, at an earlier time point than differences were detected with BLI (Figure 6a). Furthermore, the 3D

micro-CT images provided the additional capability of quantitatively measuring femur volume normalized for growing bone length, which was critical for detecting differences between all three treatment groups (Figure 6b). This was possible despite the fact that the anti-c-fms antibody treatment was only given once, allowing surviving tumor cells in bone the opportunity to grow and cause bone destruction. This improvement offered by micro-CT is offset by the longer scan times and greater cost relative to BLI, and the greater expertise required to obtain, process, and analyze high-quality micro-CT images. Yet, improvements in the automation of micro-CT image acquisitions and analyses have potential to reduce the level of expertise needed for future studies using bone metastasis models.[48]

Conclusion

Using a MDA-MB-231-BO breast cancer cell line that preferentially and reliably metastasizes to bone in an *in vivo* murine model, anti-human c-fms antibody was shown to significantly inhibit establishment of tumor cells in bone by day 7. A long-term follow-up of the effect of early one-time anti-human c-fms antibody on bone metastases and bone destruction demonstrated a lag in growth, along with inhibition of extent of bone metastasis and bone destruction. These long-term effects were demonstrated with *in vivo* BLI and micro-CT imaging, with more statistically significant results achieved with micro-CT. These results suggest that neutralizing c-fms on the human breast cancer cell by a simple one-time antibody-based approach may impact significantly on growth rate of bone metastases and on extent of bone destruction.

Authors Contributions: SKC conceived and designed the research project and provided study supervision; JJ, MDP, and SKC developed the methodology, acquisition, analysis, and interpretation of data, writing, review, and revision of the manuscript; KL provided immunohistochemical analysis and interpretation, helped with in vivo experiments, and acquisition of data; KL and HW provided cell and reagent preparations; JV, WH, and NA contributed analysis and interpretation of data; SG performed acquisition of data.

ACKNOWLEDGEMENTS

The authors thank Drs Patrick Mantyh and Anne Cress for their insightful discussions. The authors also thank Roche Diagnostics GmbH, Penzberg, Germany for providing the relevant antibodies. This study is supported by Arizona Biomedical Research Commission (to SKC), Better than Ever grant (to SKC), Rodel Foundation (to SKC), Women's Cancers of the University of Arizona Cancer Center, and the Cancer Imaging, Experimental Mouse, and Tissue Acquisition and Cellular/Molecular Analysis Shared Services of the University of Arizona Cancer Center, that are supported by the Arizona Cancer Center Support Grant, NIH P30 CA023074. This work was also supported by NIH R01CA167183.

REFERENCES

1. Clohisy DR, Palkert D, Ramnaraine ML, Pekurovsky I, Oursler MJ. Human breast cancer induces osteoclast activation and increases the number of osteoclasts at sites of tumor osteolysis. *J Orthop Res* 1996;**14**:396–402
2. Ramnaraine ML, Mathews WE, Donohue JM, Lynch CM, Goblirsch MJ, Clohisy DR. Osteoclastsdirect bystander killing of bone cancer. *Cancer Res* 2006;**66**:10929–35
3. Mancino AT, Klimberg VS, Yamamoto M, Manolagas SC, Abe E. Breast cancer increases osteoclastogenesis by secreting M-CSF and upregulating RANKL instromal cells. *J Surg Res* 2001;**100**:18–24
4. Fuller K, Owens JM, Jagger CJ, Wilson A, Moss R, Chambers TJ. Macrophage colony-stimulating factor stimulates survival and chemotactic behavior in isolated osteoclasts. *J Exp Med* 1993;**178**:1733–44
5. Feng X, Takeshita S, Namba N, Wei S, Teitelbaum SL, Ross FP. Tyrosines 559 and 807 in the cytoplasmic tail of the macrophage colony-stimulating factor receptor play distinct roles in osteoclast differentiation and function. *Endocrinology* 2002;**143**:4868–74
6. Kingsley LA, Fournier PGJ, Chirgwin JM, Guise TA. Molecular biology of bone metastasis. *Mol Cancer Ther* 2007;**6**:2609–17
7. Mantyh PW. Cancer pain and its impact on diagnosis, survival and quality of life. *Nat Rev Neurosci* 2006;**l7**:797–809
8. Maher MG, Sapi E, Turner B, Gumbs A, Perrotta PL, Carter D, Kacinski BM, Haffty BG. Prognostic significance of colony-stimulating factor receptor expression in ipsilateral breast cancer recurrence. *Clin Cancer Res* 1998;**4**:1851–6
9. Kluger HM, Dolled-Filhart M, Rodov S, Kacinski BM, Camp RL, Rimm DL. Macrophage colony-stimulating factor-1 receptor expression is associated with poor outcome in breast cancer by large cohort tissue microarray analysis. *Clin Cancer Res* 2004;**10**:173–7
10. Woo HH, Zhou Y, Yi X, David CL, Zheng W, Gilmore-Hebert M, Kluger HM, Ulukus ED, Baker T, Stoffer JB, Chambers SK. Regulation of non-AU-rich element containing c-fms proto-oncogene expression by HuR in breast cancer. *Oncogene* 2009;**28**:1176–86
11. Woo HH, Yi X, Lamb T, Menzl I, Baker T, Shapiro DJ, Chambers SK. Post-transcriptional suppression of proto-oncogene c-fms expression by vigilin in breast cancer. *Mol Cell Biol* 2011;**31**:215–25
12. Filderman AE, Bruckner A, Kacinski BM, Deng N, Remold HG. Macrophage colony-stimulating factor (CSF-1) enhances invasiveness in CSF-1 receptor-positive carcinoma cell lines. *Cancer Res* 1992;**52**:3661–6
13. Toy EP, Bonafe N, Savlu A, Zeiss C, Zheng W, Flick M, Chambers SK. Correlation of tumor phenotype with c-fms proto-oncogene expression in an in vivo intraperitoneal model for experimental human breast cancer metastasis. *Clin Exp Metastasis* 2005;**22**:1–9
14. Toy EP, Lamb T, Azodi M, Roy WJ, Woo HH, Chambers SK. Inhibition of the c-fms proto-oncogene autocrine loop and tumor phenotype in glucocorticoid stimulated human breast carcinoma cells. *Breast Cancer Res Treat* 2011;**129**:411–9
15. Sapi E, Flick MB, Rodov S, Gilmore-Hebert M, Kelley M, Rockwell S, Kacinski BM. Independent regulation of invasion and anchorage-independent growth by different autophosphorylation sites of the macrophage colony-stimulating factor 1 receptor. *Cancer Res* 1996;**56**:5704–12
16. Kacinski BM, Scata KA, Carter D, Yee LD, Sapi E, King BL, Chambers SK, Jones MA, Pirro MH, Stanley ER, Rohrschneider LR. FMS (CSF-1 receptor) and CSF-1 transcripts and protein are expressed by human breast carcinomas in vivo and in vitro. *Oncogene* 1991;**6**:941–52
17. Flick MB, Sapi E, Perrotta PL, Maher MG, Halaban R, Carter D, Kacinski BM. Recognition of activated CSF-1 receptor in breast carcinomas by a tyrosine 723 phosphospecific antibody. *Oncogene* 1997;**14**:2553–61
18. Scholl SM, Mosseri V, Tang R, Pouillart P. Expression of colony stimulating factor-1 and its receptor (the protein product of c-fms) in invasive breast tumor cells. *Ann NY Acad Sci* 1993;**698**:131–5
19. Borycki AG, Smadja F, Stanley R, Leibovitch SA. Colony-stimulating factor 1 (CSF-1) is involved in an autocrine growth control of rat myogenic cells. *Exp Cell Res* 1995;**218**:213–22

20. Patsialou A, Wyckoff J, Wang Y, Goswami S, Stanley ER, Condeelis JS. Invasion of human breast cancer cells in vivo requires both paracrine and autocrine loops involving the colony-stimulating factor-1 receptor. *Cancer Res* 2009;**69**:9498–506
21. Wrobel CN, Debnath J, Lin E, Beausoleil S, Roussel MF, Brugge JS. Autocrine CSF-1R activation promotes Src-dependent disruption of mammary epithelial architecture. *J Cell Biol* 2004;**165**:263–73
22. Pollard JW. Tumour-educated macrophages promote tumour progression and metastasis. *Nat Rev Cancer* 2004;**4**:71–8
23. Goswami S, Sahai E, Wyckoff JB, Cammer M, Cox D, Pixley FJ, Stanley ER, Segall JE, Condeelis JS. Macrophages promote the invasion of breast carcinoma cells via a colony-stimulating factor-1/epidermal growth factor paracrine loop. *Cancer Res* 2005;**65**:5278–83
24. Pollard JW. Trophic macrophages in development and disease. *Nat Rev Immunol* 2009;**9**:259–70
25. Hernandez L, Smirnova T, Kedrin D, Wyckoff J, Zhu L, Stanley ER, Cox D, Muller WJ, Pollard JW, Van Rooijen N, Segall JE. The EGF/CSF-1 paracrine invasion loop can be triggered by heregulin ß1 and CXCL12. *Cancer Res* 2009;**69**:3221–7
26. Lin EY, Nguyen AV, Russell RG, Pollard JW. Colony-stimulating factor 1 promotes progression of mammary tumors to malignancy. *J Exp Med* 2001;**193**:727–40
27. Paulus P, Stanley ER, Schafer R, Abraham D, Aharinejad S. Colony-stimulating factor-1 antibody reverses chemoresistance in human MCF-7 breast cancer xenografts. *Cancer Res* 2006;**66**:4349–56
28. Aharinejad S, Paulus P, Sioud M, Hofmann M, Zins K, Schafer R, Stanley ER, Abraham D. Colony-stimulating factor-1 blockade by antisense oligonucleotides and small interfering RNAs suppresses growth of human mammary tumor xenografts in mice. *Cancer Res* 2004;**64**:5378–84
29. Cecchini MG, Hofstetter W, Halasy J, Wetterwald A, Felix R. Role of CSF-1 in bone and bone marrow development. *Mol Reprod Dev* 1997;**46**:75–84
30. Murray LJ, Abrams TJ, Long KR, Ngai TJ, Olson LM, Hong W, Keast PK, Brassard JA, O'Farrell AM, Cherrington JM, Pryer NK. SU11248 inhibits tumor growth and CSF-1R-dependent osteolysis in an experimental breast cancer bone metastasis model. *Clin Exp Metastasis* 2003;**20**:757–66
31. Hiraga T, Nakamura H. Imatinibmesylate suppresses bone metastases of breast cancer by inhibiting osteoclasts through the blockade of c-Fms signals. *Int J Cancer* 2009;**124**:215–22
32. Manthey CL, Johnson DL, Illig CR, Tuman RW, Zhou Z, Baker JF, Chaikin MA, Donatelli RR, Franks CF, Zeng L, Crysler C, Chen Y, Yurkow EJ, Boczon L, Meegalla SK, Wilson KJ, Wall MJ, Chen J, Ballentine SK, Ott H, Baumann C, Lawrence D, Tomczuk BE, Molloy CJ. JNJ-28312141, a novel orally active colony-stimulating factor-1 receptor/FMS-related receptor tyrosine kinase-3 receptor tyrosine kinase inhibitor with potential utility in solid tumors, bone metastases, and acute myeloid leukemia. *Mol Cancer Ther* 2009;**8**:3151–61
33. Ohno H, Kubo K, Murooka H, Kobayashi Y, Nishitoba T, Shibuya M, Shibuya M, Isoe T. A c-fms tyrosine kinase inhibitor, Ki20227, suppresses osteoclast differentiation and osteolytic bone destruction in a bone metastasis model. *Mol Cancer Ther* 2006;**5**:2634–43
34. Yoneda T, Williams PJ, Hiraga T, Niewolna M, Nishimura R. A bone-seeking clone exhibits different biological properties from the MDA-MB-231 parental human breast cancer cells and a brain-seeking clone in vivo and in vitro. *J Bone Miner Res* 2001;**16**:1486–95
35. Mundy GR. Metastasis to bone: causes, consequences and therapeutic opportunities. *Nat Rev Cancer* 2002;**2**:584–93
36. Kang Y, Siegel PM, Shu W, Drobnjak M, Kakonen SM, Cordón-Cardo C, Guise TA, Massaqué J. A multigenic program mediating breast cancer metastasis to bone. *Cancer Cell* 2003;**3**:537–49
37. Wetterwald A, van der Pluijm G, Que I, Sijmons B, Buijs J, Karperien M, Löwik CW, Gautschi E, Thalmann GN, Cecchini MG. Optical imaging of cancer metastasis to bone marrow: a mouse model of minimal residual disease. *Am J Pathol* 2002;**160**:1143–53
38. Baggett B, Roy R, Momen S, Morgan S, Tisi L, Morse D, Gillies RJ. Thermostability of firefly luciferases affects efficiency of detection by in vivo bioluminescence. *Mol Imaging* 2004;**3**:324–32
39. Phadke PA, Mercer RR, Harms JF, Jia Y, Frost AR, Jewell JL, Bussard KM, Nelson S, Moore C, Kappes JC, Gay CV, Mastro AM, Welch DR. Kinetics of metastatic breast cancer cell trafficking in bone. *Clin Cancer Res* 2006;**12**:1431–40
40. Kaijzel EL, van der Pluijm G, Löwik CW. Whole-body optical imaging in animal models to assess cancer development and progression. *Clin Cancer Res* 2007;**13**:3490–7
41. Lim E, Modi K, Christensen A, Meganck J, Oldfield S, Zhang N. Monitoring tumor metastases and osteolytic lesions with bioluminescence and micro CT imaging. *J Vis Exp* 2011;**50**:e2775
42. Buie HR, Campbell GM, Klinck RJ, MacNeil JA, Boyd SK. Automatic segmentation of cortical and trabecular compartments based on a dual threshold technique for in vivo micro-CT bone analysis. *Bone* 2007;**41**:505–15
43. Gielkens PFM, Schortinghuis J, de Jong JR, Huysmans MCDNJM, van Leeuwen MBM, Raghoebar GM, Box RR, Stegenga B. A comparison of micro-CT, microradiography and histomorphometry in bone research. *Arch Oral Biol* 2008;**53**:558–66
44. Chambers SK, Kacinski BM, Ivins CM, Carcangiu ML. Overexpression of epithelial macrophage colony-stimulating factor (CSF-1) and CSF-1 receptor: a poor prognostic factor in epithelial ovarian cancer, contrasted with a protective effect of stromal CSF-1. *Clin Cancer Res* 1997;**3**:999–1007
45. Wyckoff JB, Wang Y, Lin EY, Li J, Goswami S, Stanley ER, Segall JE, Pollard JW, Condeelis J. Direct visualization of macrophage-assisted tumor cell intravasation in mammary tumors. *Cancer Res* 2007;**67**:2649–56
46. Qian B, Deng Y, Im JH, Muschel RJ, Zou Y, Li J, Lang RA, Pollard JW. A distinct macrophage population mediates metastatic breast cancer cell extravasation. *PLoS ONE* 2009;**4**:e6562
47. Cowey S, Szafran AA, Kappes J, Zinn KR, Siegal GP, Desmond RA, Kim H, Evans L, Hardy RW. Breast cancer metastasis to bone: evaluation of bioluminescent imaging and microSPECT/CT for detecting bone metastasis in immunodeficient mice. *Clin Exp Metastasis* 2007;**24**:389–401
48. Baiker M, Snoeks TJA, Kaijzel EL, Que I, Dijkstra J, Lelieveldt BP, Löwik CW. Automated bone volume and thickness measurements in small animal whole-body MicroCT data. *Mol Imaging Biol* 2012;**14**:420–30

(Received July 30, 2013, Accepted December 9, 2013)